



# Method of recognizing sleep postures based on air pressure sensor and convolutional neural network: For an air spring mattress

Yao Chao <sup>a,1</sup>, Tao Liu <sup>b,2</sup>, Li-Ming Shen <sup>a,\*</sup>

<sup>a</sup> College of Furnishings and Industrial Design, Nanjing Forestry University, Nanjing, 210037, PR China

<sup>b</sup> College of Information Science and Technology, Nanjing Forestry University, Nanjing, 210037, PR China



## ARTICLE INFO

### Keywords:

Sleep postures recognition

Air pressure sensor

Convolutional neural network

Air spring mattress

## ABSTRACT

The present study aimed to develop a sleep postures recognition system based on the hardness adjustment system for a specific air spring mattress. To the end, an air spring mattress prototype and its embedded system was manufactured. Then the supine and lateral postures were defined, and the sleep posture images generated by the relative change rate of air pressure matrix were filtered. At last, a convolutional neural network (CNN) model was proposed and analyzed by ablation experiment. Furthermore, the CNN model was compared with a CNN-SVM fusion model and a ResNet50 model to validate the performance. The results indicate that it is feasible to define sleep postures with the air pressure, and the images smoothed by a Gaussian filter contains significant features. The F1-score of the CNN model determined by the ablation experiment is 0.981, while the F1-score values of the CNN-SVM fusion model and the ResNet50 model are 0.932 and 0.954, respectively. Therefore, the generalization ability of the CNN model proposed outperformed the other two. Finally, the F1-score of the SSA-CNN model optimized by Sparrow Search Algorithm (SSA) increased to 0.992. It concludes that sleep posture recognition can be achieved using only the inherent structure of the air spring mattress without additional sensors, reducing the cost and complexity of the system. In addition, the air pressure signal can be processed by the proposed CNN model to recognize sleep postures with a high accuracy.

## 1. Introduction

Human beings spend approximately a third of their lives on mattresses, which plays a crucial role in physical and mental health. The hardness of a mattress affects not only the pressure distribution of the human-mattress interface (Yu et al., 2021) but also the spinal alignment (Park et al., 2009; Verhaert et al., 2012; Lee et al., 2019; Yu-Chi et al., 2020). Therefore, the ideal mattress should be able to adjust the hardness based on the spinal alignment. The use of active adjustment units, such as air springs (Chao and Shen, 2022) and air cells (Lee et al., 2019), makes it possible.

Furthermore, spinal alignment varies in different sleep postures (SPs) and requires different support. Specifically, the spinal alignment should be similar in the sagittal plane to that of a natural standing posture in the supine posture and straight in the coronal plane in the lateral posture. Therefore, an intelligent mattress must recognize the SPs.

Current SP recognition and mattress regulation systems are implemented through different hardware and sensors, increasing the complexity of the overall system and the number of sensors. In addition,

the current intelligent mattress structure is mainly designed to relieve pressure distribution at the human-mattress interface. It cannot precisely adjust the mattress hardness in different areas according to the spinal alignment in the SPs.

The key idea to overcome these challenges is to develop a SP function based on the hardness regulation systems of a mattress. An air spring mattress and embedded control system have been proposed, which adopt air pressure sensors to classify SPs and control the hardness.

In particular, the system: (1) collects the equilibrium air pressure through the air pressure sensors; (2) analyzes the signal through the STM32 chip to judge the SP and the hardness of the mattress; (3) finally, sends commands to the actuator to adjust the hardness.

The main contributions of this paper are as follows:

- (1) A prototype air spring mattress is proposed, which can recognize the SPs and actively adjust the mattress hardness. The SP recognition and the hardness adjustment systems share the same hardware configuration and actuators, reducing the system's complexity.

\* Correspondence to: College of Furnishings and Industrial Design, Nanjing Forestry University, No. 159 Longpan Road, Nanjing, 210037, Jiangsu, PR China.  
E-mail addresses: [chaoyao@njfu.edu.cn](mailto:chaoyao@njfu.edu.cn) (Y. Chao), [lt0906@njfu.edu.cn](mailto:lt0906@njfu.edu.cn) (T. Liu), [shenlm@njfu.edu.cn](mailto:shenlm@njfu.edu.cn) (L.-M. Shen).

<sup>1</sup> College of Furnishings and Industrial Design, Nanjing Forestry University, No. 159 Longpan Road, Nanjing, 210037, Jiangsu, PR China.

<sup>2</sup> College of Information Science and Technology, Nanjing Forestry University, No. 159 Longpan Road, Nanjing, 210037, Jiangsu, PR China.

- (2) SP are defined with the relative change rate of air pressure when a user turns over.
- (3) The SP classification model is established based on the convolutional neural network (CNN) model. It is a novel method to describe SPs using inherent sensors of the air spring mattress instead of independent sensors.

The rest of the paper is organized as follows. Section 2 reviews the related work. Section 3 presents the material and methods, including the air spring mattress prototype, experimental procedure, data processing method, and the structure of CNN SP recognition model. Section 4 evaluates the proposed CNN model and compares it with CNN-SVM fusion model and ResNet50 model. Section 5 discusses the limitations and future work. Finally, the paper concludes with Section 6.

## 2. Related work

In recent years, machine vision and deep learning models have made rich theoretical achievements in object detection and SP recognition. Among them, target detection is mainly applied in complex scenes containing multiple objects to identify specific objects and their positioning. It has comprehensive application value in the field of human-robot interaction. For example, an optimization algorithm model for accurate identification of small and medium-sized targets in variable scenarios was proposed (Huang et al., 2022a, 2021, 2022b) and further modified by reducing the number of model parameters (Yun et al., 2022). In addition, in the field of human-robot interaction, a gesture recognition system through a deep parallel network was proposed to solve the problem of real-time recognition of very complex and small hand gestures in images (Gao et al., 2019, 2020). Furthermore, the model was improved through a 3D convolutional neural network to recognize continuous gestures (Liu et al., 2021). Meanwhile, the sEMG signal of the hand can also be used to recognize gestures (Wang et al., 2022; Yang et al., 2021).

However, different from the images processed by the above target detection and gesture recognition models, the SP images generated by sensors do not include complex scenes. Therefore, the SP recognition model mainly focuses on classifying SP images generated by signals. Accordingly, in the specific research of intelligent mattress, collecting and processing signals is the key issues, which include noncontact, contact but noninvasive, and invasive means.

The noncontact means mainly includes cameras, motion sensors, and other sensors, such as sonars, radars, and thermocouples. For example, an infrared camera was used to collect SP images, which were processed by a convolutional neural network model to recognize seven SPs with an accuracy of 88.9% (Tam et al., 2021). Compared with ordinary cameras (Xia et al., 2016), infrared cameras have no privacy risk and are less affected by blankets. Moreover, the prediction accuracy can rise by over 90% with an infrared camera and a motion sensor (Deng et al., 2018), which is robust to self-occlusion. However, the effect of the blanket was present when using cameras (Mohammadi et al., 2021; Rasouli and Payandeh, 2019). In addition, the Kinect sensors have been widely used, and the algorithms are various. For one thing, Rasouli and Payandeh (2019) extracted features used to recognize the supine and lateral posture from the frequency domain of SP images. In contrast, Mohammadi et al. (2019) and Ren et al. (2020) extracted features from the original deep images training a deep learning network model. Nevertheless, the overall prediction accuracy is lower. Apart from the above, thermocouples (Chen et al., 2021), sonars (Li et al., 2021) and ultra-wideband radars (Piriyajitakonkij et al., 2021) have been applied in the nursing mattresses to recognize the SPs.

Meanwhile, although the contact means are the mainstream, including pressure sensors, acceleration sensors (Jeon et al., 2019; Roshini and Kiran, 2022), Time-of-Flying sensors (Lee et al., 2019), and potentiometers (Verhaert et al., 2011a), the pressure sensor pad is the

prevailing one. On the whole, pressure images are the prevailing input signals, but the methods of processing and extracting features are various. For example, deep neural network models were trained with the pressure image contour features (Garcia-Magarino et al., 2018; Hu et al., 2021). In contrast, (Xu et al., 2016) converted the pressure image into a topographic map based on the Body-Earth Mover's Distance and then matched six SPs by the Euclidean distance similarity. Furthermore, Kim et al. (2019) defined six SPs by pressure image features of the head, shoulder, and hip regions, which were classified by pattern matching. Additionally, Liu et al. (2014) extracted the skeleton maps from pressure images. Last but not least, a less costly miniature scale pressure mat system, half of the conventional pressure mat in size, was employed to acquire pressure images (Diao et al., 2021; Lin et al., 2002). In terms of improved algorithms, a self-supervised learning network model consisting of the upstream self-supervised training task and the downstream recognition task (Zhao et al., 2020) and a multitask neural network were proposed to improve the prediction accuracy (Vandad et al., 2020).

Although much research has provided remarkable theoretical achievements, several problems still need to be solved. (1) There are few SP recognition systems concerning household mattresses (Verhaert et al., 2012, 2011b, 2013). (2) The existing SP recognition system complicates the embedded system of the specific air spring mattress. (3) There needs to be a suitable SP recognition algorithm and model to process air pressure signal for the air spring mattress under development (Chao and Shen, 2022). Consequently, this study aims to explore a method to recognize SPs by air pressure sensors. The second purpose is to develop an air spring mattress prototype to recognize SPs and adjust hardness through the same hardware configuration.

## 3. Materials and methods

### 3.1. Air spring mattress prototype

**Fig. 1** illustrates the structure diagram of the prototype. The bedding layers contained polyurethane and latex foam with a thickness of 30 mm. In addition, the air springs were the actuator driven by air pumps. Moreover, each air spring connected a solenoid valve to form a branch air path integrated into the main air path. The air pressure sensor on the main air path measured the air pressure of each branch path when the corresponding solenoid valve turned on. The principle was that the air pressure sensors collected the air pressure and sent it to the central control unit, which received and processed the signals to control the air pumps and solenoid valves.

**Fig. 2** illustrates the structure diagram of the air paths. Air springs in the trunk region were controlled separately. To reduce the solenoid valves, the air springs in the head and leg regions were connected in series as two air paths. Therefore, air springs in the trunk region formed an 11-order matrix with 121 branch air paths. In addition, the trunk region was divided into four areas controlled by four subordinate control units, and four air pumps to inflate efficiently, as shown in different colors. Finally, the subordinate control units were controlled by the central control unit.

### 3.2. Embedded system and signal processing

#### 3.2.1. Embedded system structure

**Fig. 3** illustrates the diagram of the embedded system, containing the layers of central control unit, communication, and data processing. The main control unit layer analyzes the air pressure signal. The communication layer is the central control unit, the information exchange channel between the main control unit and the data processing layer. Moreover, the data processing layer consists of four subordinate control units, collecting the air pressure signals and controlling the solenoid valves and air pumps. **Fig. 4** illustrates the PID algorithm adjusting the output power of the air pump. It is the most mature technology in the continuous system and the most widely used control algorithm.

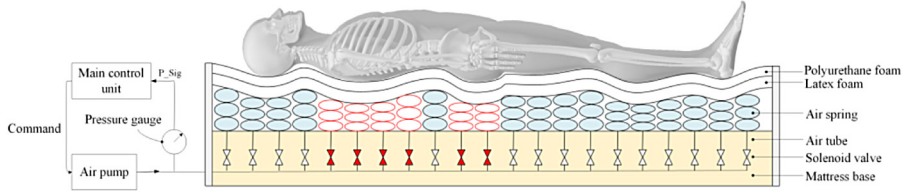


Fig. 1. Structure diagram of air spring mattress prototype.

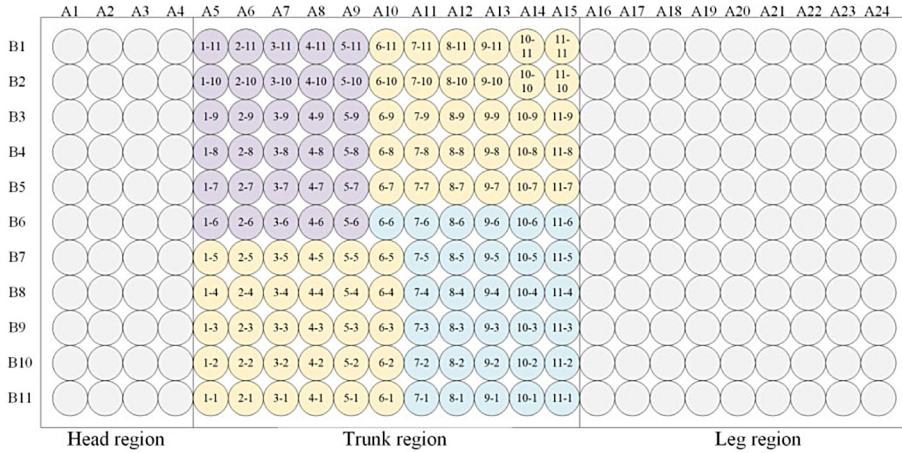


Fig. 2. Structure diagram of the air path.

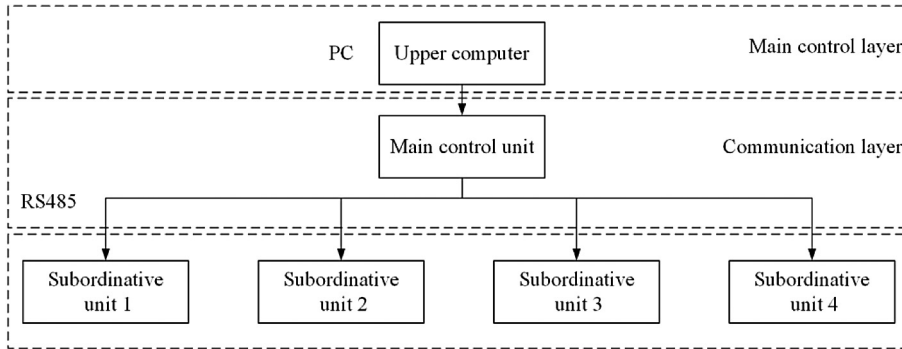


Fig. 3. Structure of the embedded system.

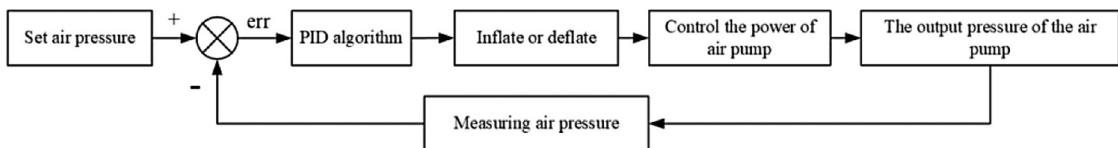


Fig. 4. The control principle of air pressure.

### 3.2.2. Hardware circuit

Fig. 5 illustrates the block diagram and some hardware of the control system. The chips of the central control unit and subordinative control unit are STM32F103RCT6 and STC15F2K60S2. The subordinative control unit collects the air pressure signal and sends it to the upper computer to recognize the real-time SPs. Then the analytical result is sent to the central control unit, which sends commands to the subordinate control units to adjust the air pressure.

The air pressure sensor (RSCM17100KP, 0–100 kPa) is made of the customized Wheatstone Bridge Varistor, which calculates the air pressure according to resistance. Four miniature air pumps with a small volume, slight noise, and considerable output air pressure are adopted. The alarm module consists of a buzzer and a LED light to remind air

leakage. The EEPROM module stores a series of personal settings for the user. The structure of the main control board is relatively simple, and the core processing unit is STM32.

### 3.3. Research process

Fig. 6 illustrates the specific research project. It contains four research modules, including SP definition based on air pressure, SP image processing, design of the CNN model and ablation experiment, comparison among different models in generalization ability and robustness, and optimal hyper-parameters of deep learning model. First, define supine and lateral postures based on the air pressure signal and

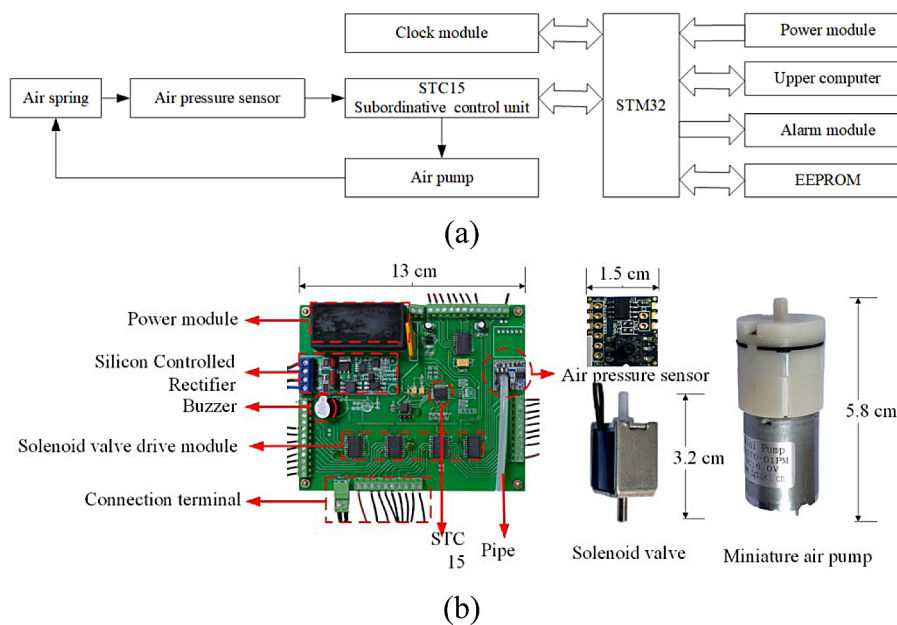


**Fig. 5.** Structure of the embedded system (a) structural block diagram, (b) subordinative control board and hardware.

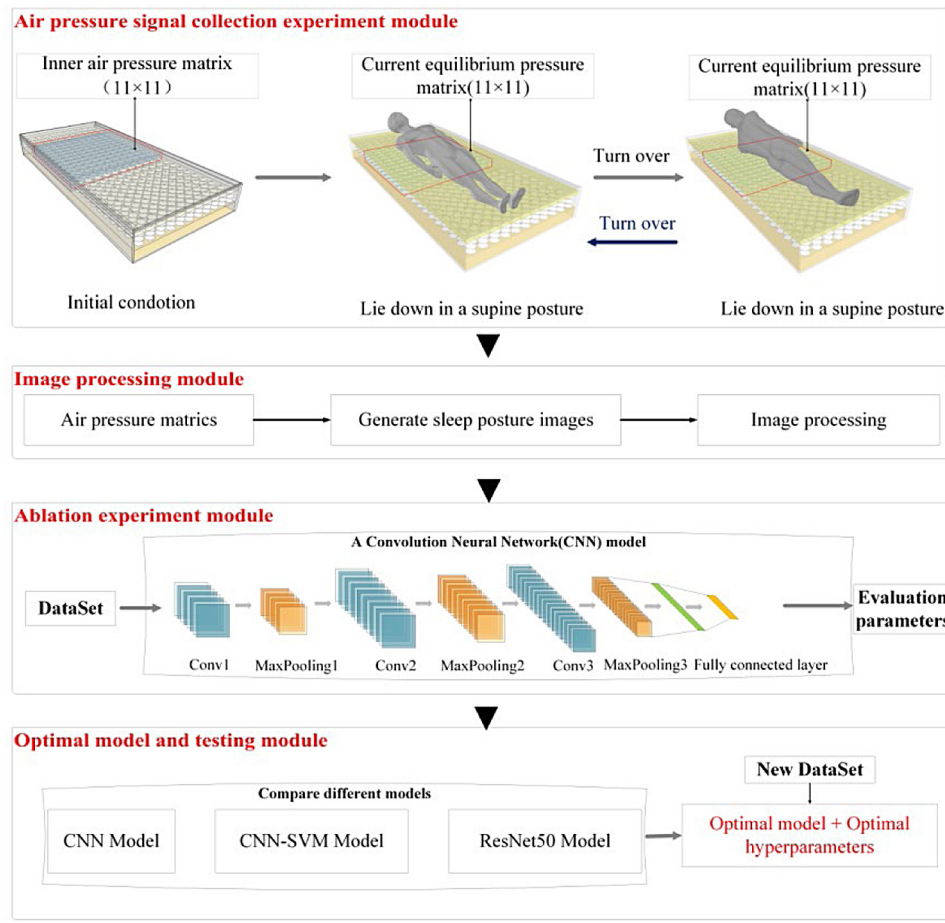


**Fig. 6.** Study flow chart.

generate SP images. Secondly, process the SP images. Then, design a CNN model and conduct the ablation experiment to determine the final structure. Furthermore, compare the generalization ability of the

proposed CNN model with a CNN-SVM fusion model and a deep residual network model ResNet50. Finally, optimize hyperparameters of the model.

**Table 1**

Basic information on subjects (Standard deviation).

Groups	Age/Years	Weight/Kg	Height/m	BMI/Kg m <sup>-2</sup>
Underweight	22 (2.53)	47.27 (5.95)	1.64 (0.08)	17.47 (0.87)
Standard	25.25 (3.01)	56.82 (4.97)	1.66 (0.06)	20.73 (1.25)
Overweight	21.71 (1.60)	78.29 (9.84)	1.73 (0.07)	26.18 (1.46)

**Table 2**

Experimental factors and levels.

Factors	Level <sup>1</sup>	Level <sup>2</sup>	Level <sup>3</sup>
A (Ratio of $P_1$ to $P_2$ )	0.5	0.7	0.9
B (Ratio of $P_2$ to $P_0$ )	1	1.3	1.5
C (Ratio of $P_3$ to $P_2$ )	0.5	0.7	0.9
D (Somatotype)	Underweight	Standard	Overweight

**Table 3**

Design of orthogonal experiment.

Column number	A	B	C	D
1	1 (0.5)	1 (1.0)	1 (0.5)	1 (Underweight)
2	1 (0.5)	2 (1.3)	2 (0.7)	2 (Standard)
3	1 (0.5)	3 (1.5)	3 (0.9)	3 (Overweight)
4	2 (0.7)	1 (1.0)	2 (0.7)	3 (Overweight)
5	2 (0.7)	2 (1.3)	3 (0.9)	1 (Underweight)
6	2 (0.7)	3 (1.5)	1 (0.5)	2 (Standard)
7	3 (0.9)	1 (1.0)	3 (0.9)	2 (Standard)
8	3 (0.9)	2 (1.3)	1 (0.5)	3 (Overweight)
9	3 (0.9)	3 (1.5)	2 (0.7)	1 (Underweight)

### 3.4. Experimental design

#### 3.4.1. Air pressure signal collection

##### (1) Subject

Since the somatypes of users affect air pressure, 26 healthy undergraduates and postgraduate students with different BMI indexes from Nanjing Forestry University were employed to increase the diversity of experimental data. Among them, there were 11 underweight subjects ( $BMI < 18.5$ , 3 males), eight normal subjects ( $18.5 \leq BMI \leq 23.9$ , 3 males), and seven overweight subjects ( $BMI > 23.9$ , 3 males). Table 1 summarizes the mean of the indexes.

##### (2) Orthogonal experimental

The air pressure signal under different conditions should be collected to increase the diversity of air pressure. To the end, divide the trunk region into the shoulder and back area, waist area, and hip area according to the body segment of each subject, and then adjust the air pressure gradient of the above areas. When a user lay down, the initial equilibrium air pressure of the waist region was set as the baseline (set as 1) and defined as  $P_0$ . Then the air pressures of the shoulder and back, waist, and hip segments were set in proportion to the baseline and defined as  $P_1$ ,  $P_2$ , and  $P_3$ . It was a four-factor and three-level experiment, shown in Table 2, and the Taguchi Orthogonal Method was used to reduce the number of experiment. Table 3 summarizes the experimental design according to the orthogonal table  $L_9(3^4)$ . Four test conditions were for each subject, including initial and three adjustment conditions, denoted as initial, M1, M2, and M3.

##### (3) Sleep postures and experimental procedure

Although there are many types of SPs, including supine, prone, and lateral postures, we only focused on the supine and lateral postures from the perspective of engineering application. Even though lateral postures consist of the fetal, the trunk, and the yearning postures, the spinal alignment does not vary depending on the positions of arms, legs, and feet. Furthermore, the mattress hardness is adjusted according to the spinal alignment in the supine and lateral postures. Therefore, the adjustment area of the air spring mattress is the trunk region, excluding the thigh area. In addition, the prone posture was not studied since it is not healthy.

**Table 4**

Hyperparameters of the CNN model.

Hyperparameters	Values	Hyperparameters	Values
miniBatchSize	128	MaxEpochs	40
InitialLearn Rate	0.001	Learn Rate Drop Period	20
LearnRateSchedule	piecewise	DropoutRate	0.2
LearnRateDropFactor	0.1	The number of neurons in fc1	128
Learn Rate Drop Period	20	The number of neurons in fc2	64

Fig. 6 illustrates the experimental procedure. Firstly, inflate the air spring to 15 kPa, and collect the equilibrium air pressure after a subject lies down in the supine posture at the initial state, defined as matrix  $P_s$ . Then record the equilibrium air pressure after the subject turns over to the lateral posture, defined as matrix  $P_L$ . Secondly, adjust the equilibrium air pressure according to Table 3. The experiment was repeated for five times for each subject until all conditions were conducted.

#### 3.4.2. CNN model and ablation experiment

Fig. 7 illustrates an initial CNN and its training weights, including three convolutional modules and three fully connected layer modules. In order to avoid overfitting, a dropout layer was added between the third convolutional layer module and the first fully connected layer module. In addition, a softmax layer and an output layer were connected after the third fully connected layer.

As shown in Fig. 7, the Conv1 of the CNN model contained 32 convolutional kernels with a size of  $3 \times 3$  and a stride of 1. The method of padding with zero was adopted to ensure that the size of feature map size remained unchanged. The number of convolutional kernels in the second and third convolutional layers was 64 and 128, respectively, and other parameters remained unchanged. In addition, the size of all maximum pooling windows was  $2 \times 2$  with a stride of 2. The solver of the CNN model was sgdm, and Table 4 summarizes hyperparameters are shown in . Furthermore, each iteration shuffles the data.

In general classification tasks, the deeper the convolutional neural network is, the better the network performance will be. Therefore, the depth of the network can be increased by increasing the convolutional and fully connected layers. In order to analyze the effect of the number of convolutional layers and the number of fully connected layers on the classification effect, an ablation experiment was conducted. Conv\_3, fc1, and fc2 were added to the model successively. The influence of the above structures on the model was evaluated according to the classification effect.

### 3.5. Model comparison

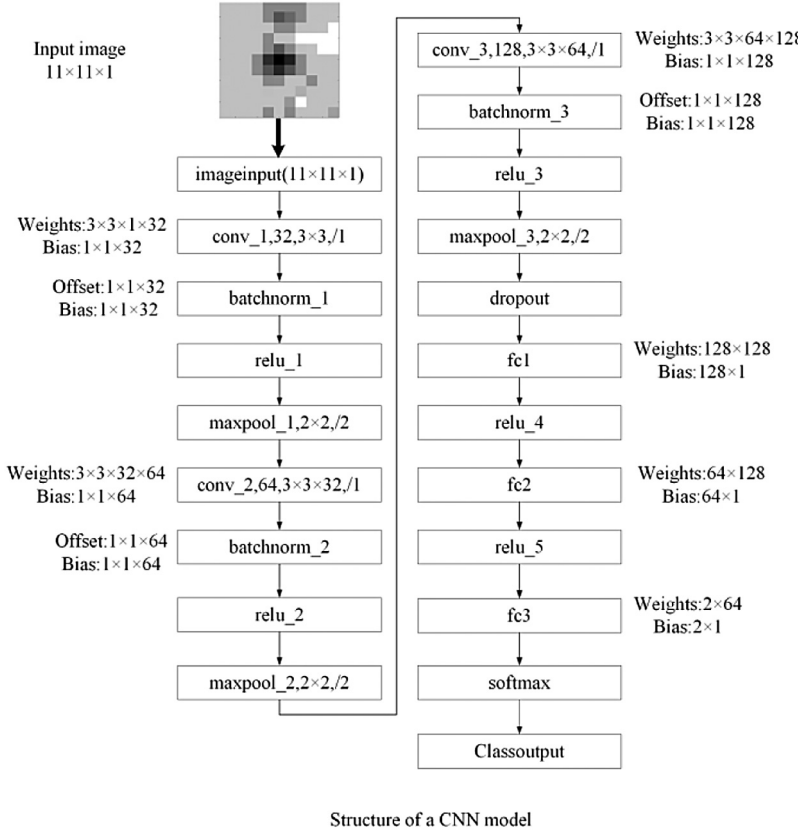
In order to compare the generalization ability and robustness of the proposed CNN model with other models, a CNN-SVM fusion model and the classical deep residual network model ResNet50 were employed. For the CNN-SVM, the feature vectors used to fit the SVM classifier were obtained by the convolutional layer of the proposed CNN model and output after processing by the last max pooling layer. For the ResNet50 model, replace the last three layers with fc1, softmax, and the classified output layer and modify the total connection layer classification number to 2 categories. Finally, the modified ResNet50 model contained 177 layers.

### 3.6. Method of data processing

#### 3.6.1. Definition of sleep postures

The equilibrium air pressure must be different after the subject turns over for the air spring mattress in any experimental condition. Based on the above principle, the relative air pressure change rate of the air springs can describe the SPs, shown in Eq. (1).

$$\begin{cases} dp_L = \frac{p_L - p_S}{p_S} \\ dp_S = \frac{p_S - p_L}{p_L} \end{cases} \quad (1)$$



Structure of a CNN model

Fig. 7. Structure of a CNN model.

where  $d_{PL}$  represents the relative change rate from the supine posture to the lateral posture, and  $d_{PS}$  represents the relative change rate from the lateral posture to the supine posture.

### 3.6.2. Sleep posture image and processing

Convert the matrix calculated by Eq. (1) into the grayscale image, whose size of the grayscale image was  $11 \times 11$  and the pixel value was between 0 and 1. However, there was noise in the raw air pressure because of the sensor accuracy, therefore, the grayscale image should be filtered to highlight the characteristics. The Gaussian and Two-dimensional adaptive filters were employed to smooth the grayscale images, and the effect of the filter types was analyzed.

The Gaussian filter is a linear filter. The value in the center position of the filer is one, and values in other positions are calculated based on the distance from the center position. The larger the distance is, the lower the weight is. For a window template whose size is  $(2k+1) \times (2k+1)$ , the value of each element in the template is calculated by Eq. (2).

$$H(i, j) = \frac{1}{2\pi\sigma^2} e^{-\frac{(i-k-1)^2-(j-k-1)^2}{2\sigma^2}} \quad (2)$$

where  $H(i, j)$  is the point coordinates and  $\sigma$  is the standard deviation.

The two-dimensional adaptive filter is a linear filter that can adapt to the local variance of the image. Therefore, the two-dimensional adaptive filter can retain more details of the original image. The local neighborhood mean and variance of each pixel in the original image are calculated as Eq. (3).

$$\begin{cases} \mu = \frac{1}{MN} \sum_{n_1, n_2 \in \eta} a(n_1, n_2) \\ \sigma^2 = \frac{1}{MN} \sum_{n_1, n_2 \in \eta} a^2(n_1, n_2) - \mu^2 \end{cases} \quad (3)$$

where  $a(n_1, n_2)$  is the pixel value of each point in the original image,  $\mu$  is the mean value, and  $\sigma$  is the variance.  $\eta$  is the  $M \times N$  local neighborhood of each pixel in the image. The algorithm of the two-dimensional adaptive filter is

$$b(n_1, n_2) = \mu + \frac{\sigma^2 - v^2}{\sigma^2} [a(n_1, n_2) - \mu] \quad (4)$$

where  $b(n_1, n_2)$  is the pixel value after two-dimensional adaptive filtering, and  $v^2$  is the noise variance. If the noise variance is not specified, the mean of all local estimated variances is used to replace the noise variance.

### 3.6.3. Evaluation indexes of deep learning model

In deep learning, the learning curve is generally used to judge whether the model is underfitting, regular fitting, or overfitting. The indexes of Accuracy, Precision, Recall/Sensitivity, and Specificity were used to evaluate the performance of a model. Moreover, the previous indexes were fused to define composite indicators, including BalanceAccuracy, F-measure, F1-score, and Matthews Correlation Coefficient (MCC).

### 3.7. Making dataset

Two datasets were produced in this study, one was used to train the model, and the other was used to test the generalization ability and robustness. The initial Train Dataset generated according Section 3.4.1 contains 1040 images, and then it was enlarged to 2080 by the left and right flips. The Train Dataset was randomly divided into a training set and a validation set according to a 0.7 ratio.

In addition, 33 subjects with different BMI values were employed to generate the Test Dataset according to Section 3.4.1. Furthermore, the grayscale images were flipped left and right and rotated randomly between  $-10^\circ$  and  $10^\circ$  to expand the sample size. Finally, 132 supine posture images and 132 lateral posture images were in the test dataset.

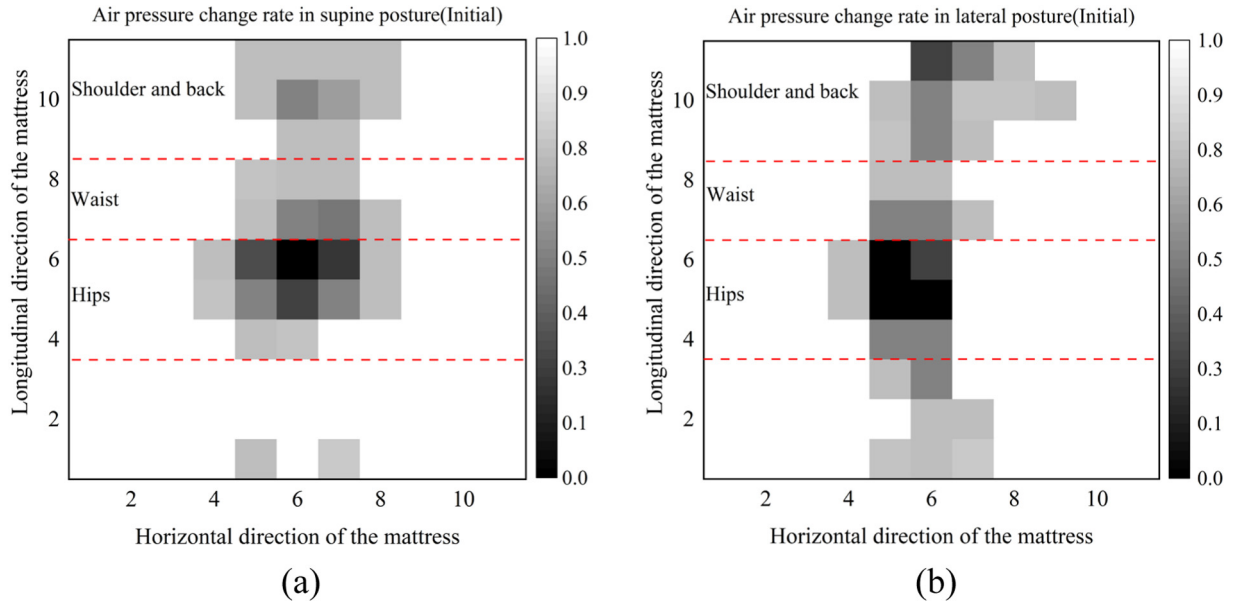


Fig. 8. Sleep posture images at the initial state.

**Table 5**

Air pressure distribution (kPa).

Experimental mode	Back region	Waist region	Hip region
M1	8	21	11
M2	11	24	8
M3	14	16	14

## 4. Results and analysis

### 4.1. Sleep posture grayscale image

Take the example of a female subject with a standard somatotype. Firstly, inflate the air spring mattress to 15 kPa at the initial condition. Then measure the inner air pressure in the supine and lateral postures, defined as  $P_S$  and  $P_L$ , respectively. Secondly, calculate the change rate of air pressure according to Eq. (1). Fig. 8 illustrates the SPs images at the initial state.

Fig. 8 (left) illustrates the supine posture, where the shoulder, waist, and hip regions were significant. Fig. 7 (right) illustrates the left lateral posture. The following difference could be seen by comparing the characteristics of the two images.

- (1) The supine posture image was larger than the lateral one in the area because the back contour was significantly larger than the side contour in the area.
- (2) The maximum pixel value of the shoulder area in the lateral posture was significantly larger than that in the supine posture because the shoulder was supported by fewer air springs in the former posture. Therefore, the load of single air spring increased, causing the increasing air pressure.
- (3) The maximum pixel value of the hip area in the lateral posture was more significant than that in the supine posture due to the smaller contact area and enormous load in the lateral posture.

The above analysis concludes that air pressure change rate reflects the SPs on the initial condition.

Moreover, the SP images on the condition of three experimental settings were obtained to analyze the characteristics under arbitrary conditions. Table 5 summarizes the corresponding experimental settings. Fig. 9 illustrates the SP images on the three working conditions.

Fig. 9 indicates that the features of SP images on three conditions did not reflect the trunk contour since the air pressure of each region

was even before turning over. However, the brightness features in the shoulder and hip segments were significantly different in the supine and lateral postures.

On the one hand, the maximum pixel value of the shoulder area in the supine posture was smaller than that in the lateral posture. The maximum pixel value and the location of the hip area differed from each other. Besides, the brightness of the grayscale images was different in different SPs. Although the difference is hard to be recognized by human eyes, it can be recognized by a computer.

Consequently, the SPs described by Eq. (1) can be used for deep learning. However, they should be filtered before further application because of much noise.

### 4.2. Image filtering

The Gaussian and two-dimensional adaptive filters were employed to process the SP grayscale images. The standard deviation of the Gaussian filter was 1, namely  $\sigma = 1$ , and the size of the filter was  $3 \times 3$ . Fig. 10 illustrates the original and the filtered grayscale images of supine and lateral postures at the M1 condition.

Fig. 10 indicates that the SP grayscale images smoothed by the Gaussian filtering were too fuzzy compared with the original image. Meanwhile, it retained more details and features smoothed by the adaptive filter. That was because the Gaussian filter was a mean filtering method only considering the distance between each pixel in the neighborhood and the center point of a filtering template, but the specific values in the neighborhood. Therefore, the Gaussian filter may ignore the features of the original images, especially for some less obvious features. In contrast, although the two-dimensional adaptive filter was also linear, it adapted to the local variance of the images. When the variance of the neighborhood was significant, the filter hardly performed smoothing, retaining the potential features, but more smoothing was performed when slight. Therefore, the two-dimensional adaptive filter retained more details of the original SP images on condition M1.

Based on the above analysis, the two-dimensional adaptive filter was much more suitable for processing the SP images.

### 4.3. Performance of the CNN classifier

#### 4.3.1. Result of the ablation experiment

According to the ablation experiment, each CNN model with different structure was trained for five times. The results of evaluation

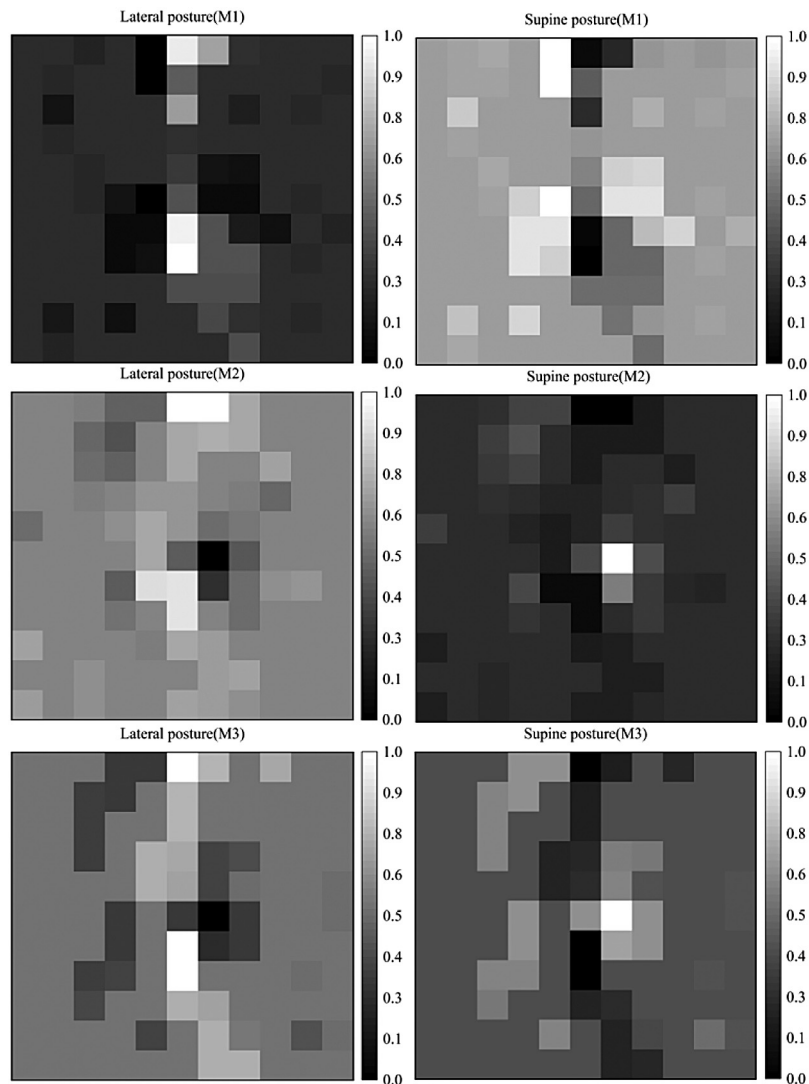


Fig. 9. Sleep posture images of three conditions.

**Table 6**  
Results of ablation experiment (Standard deviation).

	Conv3	✓	✓	✓	✓
Analytical layers	Fc1		✓		✓
	Fc2			✓	✓
Train Dataset	BalanceAccuracy	0.960 (0.004)	0.971 (0.005)	0.967 (0.009)	0.968 (0.006)
	F_measure	1.920 (0.008)	1.942 (0.010)	1.935 (0.019)	1.936 (0.012)
	F1_score	0.960 (0.004)	0.971 (0.005)	0.967 (0.009)	0.968 (0.006)
	MCC	0.919 (0.0048)	0.942 (0.010)	0.935 (0.018)	0.936 (0.012)
Test Dataset	BalanceAccuracy	0.967 (0.016)	0.986 (0.013)	0.973 (0.010)	0.974 (0.009)
	F_measure	1.935 (0.033)	1.971 (0.027)	1.947 (0.021)	1.948 (0.019)
	F1_score	0.967 (0.016)	0.985 (0.014)	0.973 (0.010)	0.974 (0.009)
	MCC	0.935 (0.032)	0.971 (0.027)	0.947 (0.021)	0.949 (0.018)

Note: ✓ represents the layer added in the CNN model.

indexes on the train and test datasets were calculated respectively, and the mean value was taken at last. Table 6 summarizes the ablation results of the proposed CNN model. The results showed that when only conv\_3 was added, the evaluation index values were the highest, indicating that the classification accuracy and the generalization ability were the best. Moreover, the slight standard deviation indicated that the training process were relatively stable. In contrast, when fc1 and fc2 were added, all the evaluation indexes in the tain and test datasets declined. Therefore, the final CNN model contained three convolution layers and one fully connected layer.

#### 4.3.2. Comparison of different models

In order to test the generalization ability of the CNN model and the differences between the CNN-SVM and ResNet50 models, the CNN model was trained and validated using the Train Dataset. After numerous training, the model with the highest classification accuracy was selected, and the maxpooling3 output feature map of this model was used as the input feature of the SVM classifier. Fig. 11 illustrates the learning curve of the CNN and ResNet50 models, and Table 7 summarizes the evaluation indexes of different models.

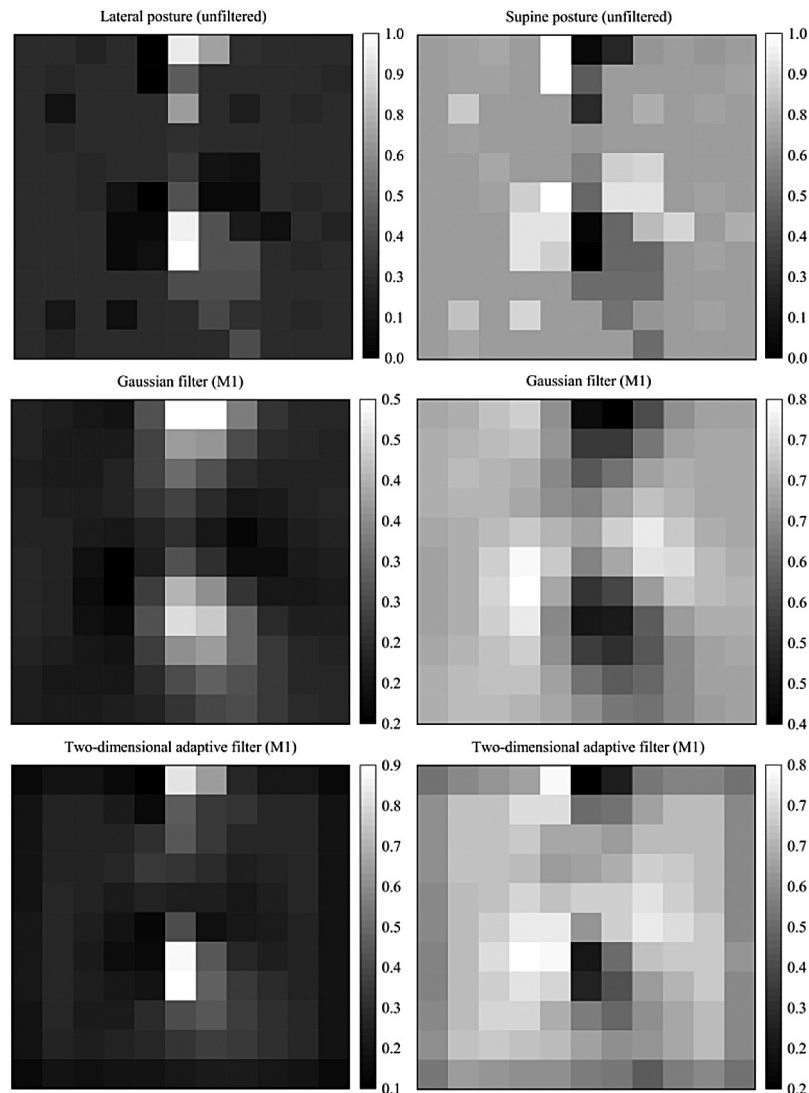


Fig. 10. Effect of filter types on the condition of M1.

**Table 7**  
Evaluation indexes of different models.

Data set	Evaluation indexes	CNN	CNN-SVM	ResNet50
Train Dataset	BalanceAccuracy	0.973	0.963	0.986
	F_measure	1.965	1.928	1.971
	F1_score	0.973	0.964	0.986
	MCC	0.946	0.927	0.971
Test Dataset	BalanceAccuracy	0.981	0.932	0.955
	F_measure	1.963	1.865	1.908
	F1_score	0.981	0.932	0.954
	MCC	0.963	0.864	0.910

Fig. 11 indicates that the training and verification Loss and Accuracy of the CNN and ResNet50 models tended to be stable with increasing iterations. The difference between the two was slight, indicating that the models were neither overfitting nor underfitting.

Table 7 shows that in the Train Dataset, the evaluation indexes of the ResNet50 were the highest among the three models, while that of the CNN-SVM model were the lowest. However, on the Test Dataset, the generalization ability of ResNet50 was inferior to that of the CNN model. Moreover, the evaluation indexes of the CNN-SVM were still the lowest among the three models, especially the MCC, only 0.86.

The above results show that the generalization ability and robustness of the CNN model were better than those of the other two models. This was because that the depth of ResNet50 was much larger than that of the CNN model, therefore, it had stronger learning ability. However, due to the noise in the SP images, which ResNet50 still learned as features, there were significant errors in the new dataset. Generally speaking, the ResNet50 model was suitable for classification tasks with large datasets. For the classification tasks in this study, it did not mean that the larger the network depth would perform well. In addition, although CNN-SVM integrated the convolutional function, it was still an SVM linear classifier, in essence, with a strict mathematical model inside. Therefore, the noise in the input high-dimensional vectors significantly impacted the classification results.

The confusion matrices of the classification of Test Dataset by different models were shown in Fig. 12. Moreover, the accuracy of the CNN, CNN-SVM, and ResNet models was 0.981, 0.932, and 0.955, respectively, and the corresponding Recall was 1, 0.939, and 0.939, respectively.

Based on the above results, the CNN model was the most suitable for the classification task of this study.

#### 4.3.3. Sparrow search algorithm optimizes CNN hyperparameters

When the structure of the CNN model remains unchanged, the hyperparameters significantly impact the training results. The minimum batch processing, the number of convolutional kernels at each

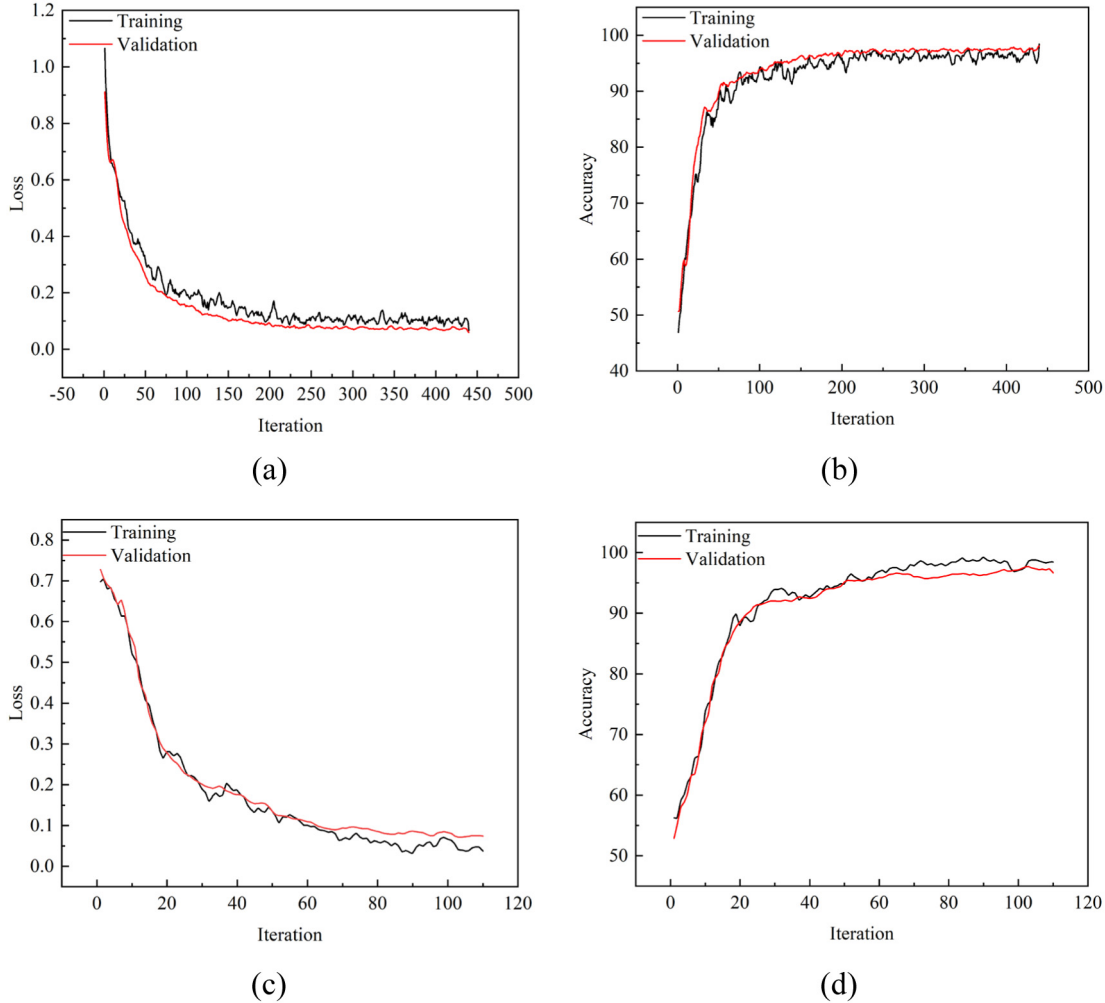


**Fig. 11.** Learning curves (a) Loss of CNN, (b) Accuracy of CNN, (c) Loss of ResNet50, (d) Accuracy of ResNet50.

**Table 8**  
Optimal hyperparameters of the CNN model.

Hyperparameters	MiniBatch Size	Number of the kernel in Conv1	Number of the kernel in Conv2	Number of the kernel in Conv3	LearnRate	Dropout rate
Value	64	32	64	128	0.01	0.25

convolutional layer, the learning rate, and the dropout rate were the hyperparameters needed optimized. In order to obtain the best combination of the above hyperparameters, the sparrow search algorithm (SSA) was employed. In the SSA algorithm, the core part was the objective function and output. In this study, the output of the objective function was the wrong classification rate of the CNN model on the Test Dataset. The smaller the wrong classification rate was, the higher the accuracy was.

Since the CNN model was trained in the objective function, and there were many cycles in the primary function of SSA, therefore, the computing cost would be very high on the condition of large population and iterations. Therefore, to reduce the running time, set the population quantity to 10 and the number of iterations to 20. Finally, the population evolution curve was shown in Fig. 13. Table 8 summarizes the optimal hyperparameters.

When the optimal hyperparameters were determined, the CNN model was trained with the best hyperparameters and Train Dataset and was evaluated with the Test Dataset after each training. After ten training sessions, Table 9 summarizes the evaluation indexes both in Train Dataset and Test Dataset. The result indicated that

the model\_2 outperformed the other models with the BalanceAccuracy and F1\_score of 0.992 and 0.992, respectively. Meanwhile, the confusion matrix and learning curves were shown in Fig. 14.

Fig. 14(a) indicated that the generalization ability of the CNN model optimized by SSA was further improved. Table 9 indicated that the BalanceAccuracy of the optimized model was 0.992, which increased by 1.12%. As a result, the CNN model could be deployed to the SP recognition system of the air spring mattress.

## 5. Discussion

The study hypothesizes that the SP recognition system can be developed with the air pressure sensors and shares the same hardware configuration with the hardness adjustment system. Based on the previous study, we designed and manufactured an air spring mattress prototype, defined the supine and lateral postures by air pressure, and trained a CNN model to recognize the two SPs with a BalanceAccuracy of 0.992. The results indicate that the recognition system can be developed based on the hardware configuration of the sleep system itself rather than by attaching external sensors and circuits to it.

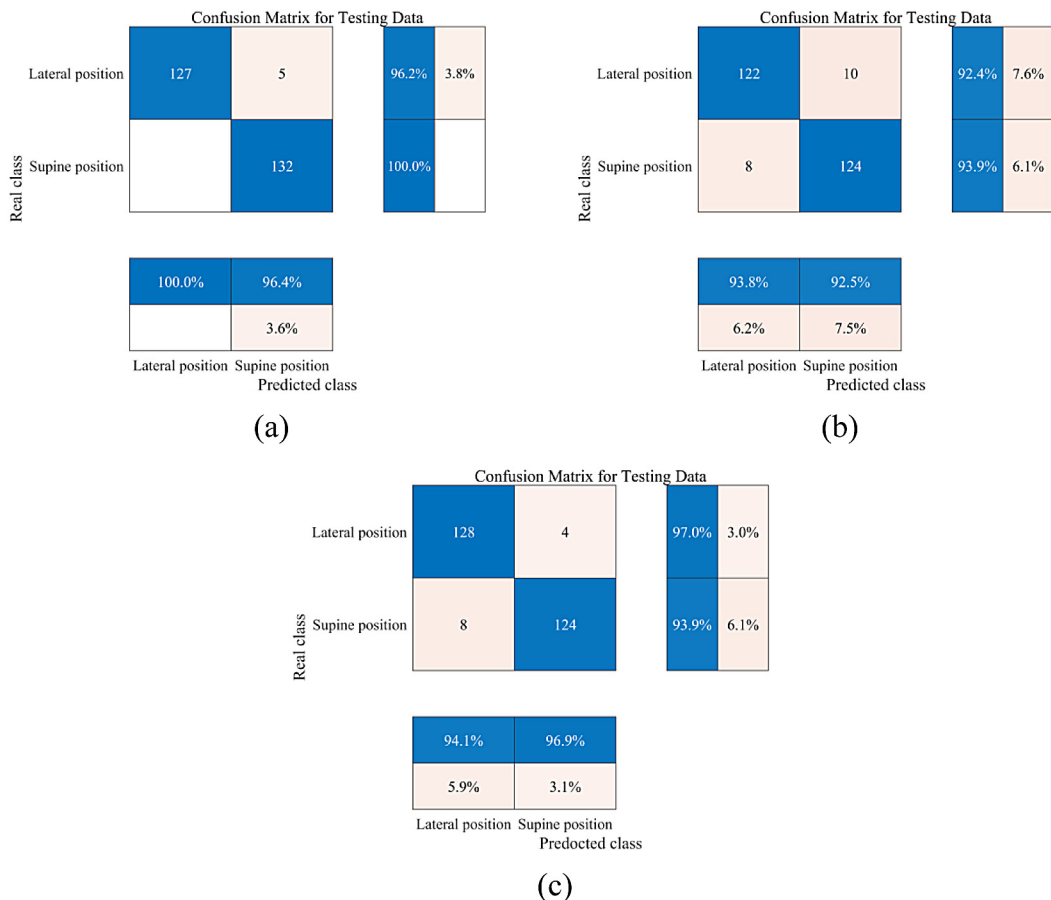


Fig. 12. Confusion matrices of Test Dataset (a) CNN model, (b) CNN-SVM model, (d) ResNet50.

**Table 9**  
Optimal hyperparameter model training process.

Evaluation indexes	Training number										
	1	2	3	4	5	6	7	8	9	10	
Train Dataset	BalanceAccuracy	0.978	0.974	0.978	0.966	0.978	0.978	0.970	0.984	0.973	0.968
	F_measure	1.955	1.949	1.955	1.932	1.955	1.955	1.938	1.968	1.945	1.935
	F1_score	0.978	0.974	0.977	0.966	0.977	0.978	0.969	0.984	0.973	0.968
	MCC	0.955	0.949	0.955	0.933	0.955	0.955	0.940	0.968	0.946	0.936
Test Dataset	BalanceAccuracy	0.981	0.992	0.989	0.992	0.970	0.973	0.981	0.977	0.973	0.951
	F_measure	1.963	1.985	1.977	1.985	1.939	1.948	1.962	1.954	1.947	1.899
	F1_score	0.981	0.992	0.989	0.992	0.970	0.974	0.981	0.977	0.973	0.949
	MCC	0.962	0.985	0.977	0.985	0.939	0.947	0.962	0.955	0.947	0.903

### 5.1. Advantages

There are two apparent advantages of the proposed method in the present study. On the one hand, the method is not affected by a blanket. In contrast, some prevalent technologies are affected, such as infrared cameras (Tam et al., 2021), depth sensors (Rasouli and Payandeh, 2019), and cameras (Xia et al., 2016). Although Mohammadi et al. (2019) disclosed that the thin blankets has little effect on infrared imaging, the influence of a thick blanket on the depth sensor remains unknown. Furthermore, Piriya JITAKONKIJ et al. (2021) explored the performance of the combination of ultra-wideband radars and deep learning with an average accuracy of 73.7%, which may not meet the engineering requirements. In contrast, the proposed CNN model in this study classifies SPs with the Balance Accuracy of 0.992.

On the other hand, the proposed SP recognition system is based on the inherent hardware configuration of the sleep system, reducing the complexity of embedded systems while saving costs. Instead, some employ other sensors independent of the sleep system, such as the

flexible pressure sensor pad (Davoodnia and Etemad, 2021; Hsiao et al., 2018; Hu et al., 2021). These SP recognition system can be used on any mattress for monitoring, but that can only recognize SPs, instead of adjusting the mattress. Meanwhile, a novel air spring and the active stiffness adjustment model for ergonomic mattresses have been proposed and tested (Chao and Shen, 2022). Therefore, we have manufactured the air spring mattress prototype based on the previous study. In the subsequent and ongoing research, we hope the air spring mattress automatically adjusts the hardness according to SPs to maintain the optimal spinal alignment. Therefore, we prefer to use the inherent air pressure sensors to develop SP recognition system in the prototype.

In terms of algorithm, learning parameters are greatly reduced and the accuracy increased by 4% of the proposed CNN model compared with the ResNet50 model, which means that the introduction of the residual module in this study does not improve the performance of the model. However, in the object detection task, an YOLO model can improve recognition by introducing a residual module (Roy et al., 2022).

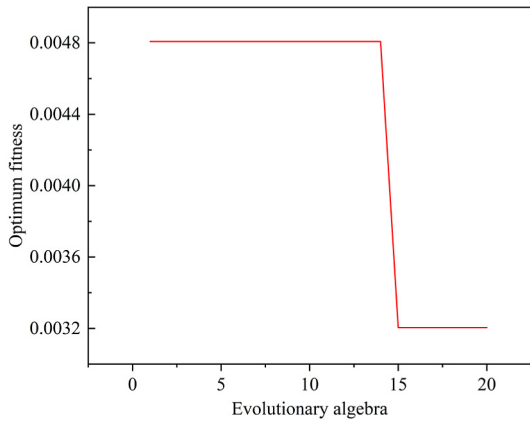


Fig. 13. Evolution curve.

The possible reason is that the SP image in this study are uncomplicated and contains noise, therefore, excessive increase of the modules and depth of the network may lead to the model taking noise as the features, thus affecting the generalization effect. Furthermore, although pseudo-examples generated by decoders in image classification may alleviate the influence of physical sample noise on training (Khan et al., 2022), it has yet to be applied in the field of SP recognition.

The ultimate goal of this research project is to develop an intelligent mattress that can automatically adjust the hardness according to the

sleep postures and spinal alignment of users. Therefore, according to the final purpose of the intelligent air spring mattress, we will solve the problem of somatotype recognition and spinal alignment measurement of users without introducing new sensors and hardware configurations. Therefore, the proposed method in the present study is ideal from the insight of the systematic research of the air spring mattress.

### 5.2. Limitations and directions for further research

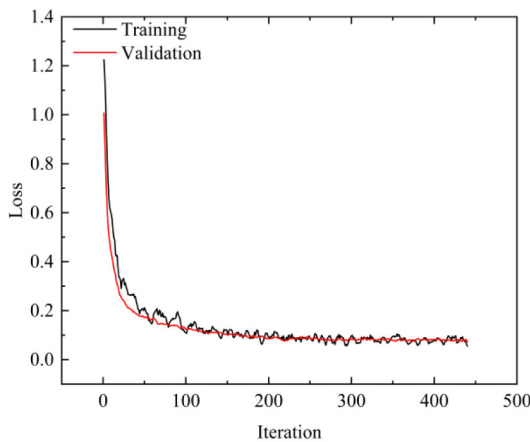
Although the results have demonstrated that an SP recognition system based on air pressure sensors can recognize the SPs with a high accuracy, some limitations must be improved. The SP recognition system only operated in a short experimental state, and the performance of overnight sleep has yet to be studied. In the following research, it is necessary to study the overnight performance of the proposed CNN model. In addition, this study only trained the sleeping posture recognition model (CNN) with static images.

In contrast, in reality, the SPs changed overnight. Therefore, SP recognition is the process of recognition of continuous SP, similar to the continuous posture recognition (Yan and Woźniak, 2022; Liu et al., 2021). In the following research, continuous SP should be further studied. Although the YOLO model, widely used in object detection at present, has high accuracy, it is mainly used to detect specific objects in complex scenes. It can solve the occlusion problem of non-specific targets (Lawal, 2021). However, it has not been applied in SP recognition. In the future studies, the YOLO model can be used to process SP images.

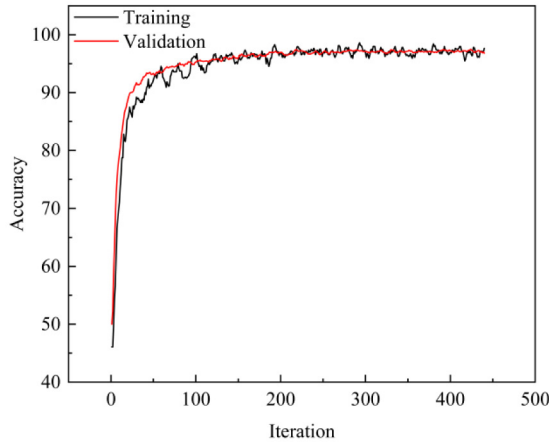
Confusion Matrix for Testing Data			
		Lateral position	Supine position
Real class	Lateral position	132	2
	Supine position	100.0%	98.5% 1.5%
		98.5%	100.0%
		1.5%	

Lateral position      Supine position  
Predicted class

(a)



(b)



(c)

Fig. 14. Learning curve of the optimal CNN model (a) confusion matrix in TestDataset, (b) Loss, (c) Accuracy.

## 6. Conclusion

This study uses an intelligent air spring mattress prototype to explore SP recognition. The following conclusions are reached.

- (1) Developing the SP recognition system through the inherent hardware configuration is feasible and less costly, reducing the complexity of the overall embedded system.
- (2) The air pressure change rate is caused by turning over the supine and lateral postures, which can be used as the input signal of deep learning after processing.
- (3) This study further expands the method of recognizing SPs based on the air pressure sensors, which could be applied to other intelligent air mattresses.
- (4) The SP image processing algorithm need further improvement to process continuous SP images

## CRediT authorship contribution statement

**Yao Chao:** Conceptualization, Methodology, Software, Formal analysis, Investigation, Writing – original draft. **Tao Liu:** Designing and manufacturing the embedded system, Completing the writing of Section 3.2. **Li-Ming Shen:** Conceptualization, Formal analysis, Writing review & editing.

## Declaration of competing interest

The authors declare that they have no known competing financial interests or personal relationships that could have appeared to influence the work reported in this paper.

## Data availability

Data will be made available on request.

## Acknowledgments

This study was supported by the Postgraduate Research and Practice Innovation Program of Jiangsu Province (KYCX20\_0859) and by the Project funded by the National First-class Disciplines (PNFD), China.

## References

- Chao, Y., Shen, L., 2022. Nonlinear stiffness characteristics and model of air spring for mattress based on finite element and numerical analysis. *Adv. Theory Simul.* 2200393. <http://dx.doi.org/10.1002/adts.202200393>.
- Chen, Z., Wang, Y., Univ, Texas A.M., T.U., C.S., 2021. Remote recognition of in-bed postures using a thermopile array sensor with machine learning. *IEEE Sens. J.* 21 (9), 10428–10436. <http://dx.doi.org/10.1109/JSEN.2021.3059681>.
- Davoodnia, V., Etemad, A., 2021. Identity and posture recognition in smart beds with deep multitask learning. In: 2019 IEEE International Conference on Systems, Man and Cybernetics. Cornell University Library, Ithaca, ArXiv.Org.
- Deng, F., Dong, J., Wang, X., Fang, Y., Liu, Y., Yu, Z., Chen, F., 2018. Design and implementation of a noncontact sleep monitoring system using infrared cameras and motion sensor. *IEEE Trans. Instrum. Meas.* 67 (7), 1555–1563. <http://dx.doi.org/10.1109/TIM.2017.2779358>.
- Diao, H., Chen, C., Yuan, W., Amara, A., Tamura, T., Fan, J., Chen, W., 2021. Deep residual networks for sleep posture recognition with unobtrusive miniature scale smart mat system. *IEEE Trans. Biomed. Circuits Syst.* 15 (1), 111–121. <http://dx.doi.org/10.1109/TBCAS.2021.3053602>.
- Gao, Q., Liu, J., Ju, Z., 2020. Robust real-time hand detection and localization for space human–robot interaction based on deep learning. *Neurocomputing* (Amsterdam) 390, 198–206. <http://dx.doi.org/10.1016/j.neucom.2019.02.066>.
- Gao, Q., Liu, J., Ju, Z., Zhang, X., 2019. Dual-hand detection for human–robot interaction by a parallel network based on hand detection and body pose estimation. *IEEE Trans. Ind. Electron.* 66 (12), 9663–9672.
- Garcia-Magarino, I., Lacuesta, R., Lloret, J., 2018. Agent-based simulation of smart beds with internet-of-things for exploring big data analytics. *IEEE Access* 6, 366–379. <http://dx.doi.org/10.1109/ACCESS.2017.2764467>.
- Hsiao, R.S., Chen, T.X., Bitew, M.A., Kao, C.H., Li, T.Y., 2018. Sleeping posture recognition using fuzzy C-means algorithm. *Biomed. Eng. Online* 17 (Suppl 2), 157. <http://dx.doi.org/10.1186/s12938-018-0584-3>.
- Hu, Q., Tang, X., Tang, W., 2021. A real-time patient-specific sleeping posture recognition system using pressure sensitive conductive sheet and transfer learning. *IEEE Sens. J.* 21 (5), 6869–6879. <http://dx.doi.org/10.1109/JSEN.2020.3043416>.
- Huang, L., Chen, C., Yun, J., Sun, Y., Tian, J., Hao, Z., Ma, H., 2022a. Multi-scale feature fusion convolutional neural network for indoor small target detection. *Front. Neurorobot.* 16, 881021. <http://dx.doi.org/10.3389/fnbot.2022.881021>.
- Huang, L., Fu, Q., He, M., Jiang, Du., Hao, Z., 2021. Detection algorithm of safety helmet wearing based on deep learning, concurrency and computation practice and experience. *Concurr. Comput. Pract. Exp.* e6234.
- Huang, L., Xiang, Z., Yun, J., Sun, Y., Liu, Y., Jiang, D., Yu, H., 2022b. Target detection based on two-stream convolution neural network with self-powered sensors information. *IEEE Sens. J.* 1, <http://dx.doi.org/10.1109/JSEN.2022.3220341>.
- Jeon, S., Park, T., Paul, A., Lee, Y., Son, S.H., 2019. A wearable sleep position tracking system based on dynamic state transition framework. *IEEE Access* 7 (1), <http://dx.doi.org/10.1109/ACCESS.2019.2942608>.
- Khan, W., Raj, K., Kumar, T., Roy, A.M., Luo, B., 2022. Introducing Urdu digits dataset with demonstration of an efficient and robust noisy decoder-based pseudo example generator. *Symmetry (Basel)* 14 (10), 1976. <http://dx.doi.org/10.3390/sym14101976>.
- Kim, T., Kwon, S., Choi, H., Hong, Y., 2019. Determination of lying posture through recognition of multiliter body parts. *Wirel. Commun. Mob. Comput.* 29, 9568584. <http://dx.doi.org/10.1155/2019/9568584>.
- Lawal, M.O., 2021. Tomato detection based on modified YOLOv3 framework. [Journal Article; Research Support, Non-U.S. Gov'T]. *Sci. Rep.* 11 (1), 1447. <http://dx.doi.org/10.1038/s41598-021-81216-5>.
- Lee, K.H., Kwon, Y.E., Lee, H., Lee, Y., Seo, J., Kwon, O., Lee, D., 2019. Active body pressure relief system with time-of-flight optical pressure sensors for pressure ulcer prevention. *Sensors (Basel)* 19 (18), <http://dx.doi.org/10.3390/s19183862>.
- Li, T., Wu, Y., Wu, F., Mohammed, S., Wong, R.K., Ong, K., 2021. Sleep pattern inference using IoT sonar monitoring and machine learning with Kennard-stone balance algorithm. *Comput. Electr. Eng.* 93, 107181. <http://dx.doi.org/10.1016/j.compeleceng.2021.107181>.
- Lin, J., Chiou, W., Weng, H., Tsai, Y., Liu, T., 2002. Comparison of three-dimensional anthropometric body surface scanning to waist-hip ratio and body mass index in correlation with metabolic risk factors. *J. Clin. Epidemiol.* 55 (8), 757–766. [http://dx.doi.org/10.1016/S0895-4356\(02\)00433-X](http://dx.doi.org/10.1016/S0895-4356(02)00433-X).
- Liu, Y., Jiang, D., Duan, H., Sun, Y., Li, G., Tao, B., Ahmed, S.H., 2021. Dynamic gesture recognition algorithm based on 3D convolutional neural network. *Comput. Intell. Neurosci.* 2021, 1–12. <http://dx.doi.org/10.1155/2021/4828102>.
- Liu, J.J., Xu, W., Huang, M., Alshurafa, N., Sarrafzadeh, M., Raut, N., Yadegar, B., 2014. Sleep posture analysis using a dense pressure sensitive bedsheet. *Pervasive Mob. Comput.* 10, 34–50. <http://dx.doi.org/10.1016/j.pmcj.2013.10.008>.
- Mohammadi, S.M., Enshaeifar, S., Hilton, A., Dijk, D.J., Wells, K., 2021. Transfer learning for clinical sleep pose detection using a single 2D IR camera. *IEEE Trans. Neural Syst. Rehabil. Eng.* 29, 290–299. <http://dx.doi.org/10.1109/TNSRE.2020.3048121>.
- Mohammadi, S.M., Kouchaki, S., Khan, S., Dijk, D.J., Hilton, A., Wells, K., 2019. Two-step deep learning for estimating human sleep pose occluded by bed covers. *Annu. Int. Conf. IEEE Eng. Med. Biol. Soc.* 2019, 3115–3118. <http://dx.doi.org/10.1109/EMBC.2019.8856873>.
- Park, S.J., Kim, J.S., Kim, C., 2009. Comfort evaluation and bed adjustment according to sleep positions. *Hum. Factors Ergon. Manuf.* 19 (2), 145–157. <http://dx.doi.org/10.1002/hfm.20142>.
- Piriyajitakonkij, M., Warin, P., Lakhan, P., Leelaarporn, P., Kumchaiseemak, N., Suwajanakorn, S., Wilaiprasitporn, T., 2021. SleepPoseNet: Multi-view learning for sleep postural transition recognition using UWB. *IEEE J. Biomed. Health Inform.* 25 (4), 1305–1314. <http://dx.doi.org/10.1109/JBHI.2020.3025900>.
- Rasouli, M.S., Payandeh, S., 2019. A novel depth image analysis for sleep posture estimation. *J. Ambient Intell. Humaniz. Comput.* 10 (5), 1999–2014. <http://dx.doi.org/10.1007/s12652-018-0796-1>.
- Ren, W., Ma, O., Ji, H., Liu, X., 2020. Human posture recognition using a hybrid of fuzzy logic and machine learning approaches. *IEEE Access* 8, 135628–135639. <http://dx.doi.org/10.1109/ACCESS.2020.3011697>.
- Roshini, A., Kiran, K., 2022. An enhanced posture prediction-Bayesian network algorithm for sleep posture recognition in Wireless Body Area networks. *Int. J. Telemed. Appl.* 2022, 3102545. <http://dx.doi.org/10.1155/2022/3102545>.
- Roy, A.M., Bhaduri, J., Kumar, T., Raj, K., 2022. WilDect-YOLO: An efficient and robust computer vision-based accurate object localization model for automated endangered wildlife detection. *Ecol. Inform.* 101919. <http://dx.doi.org/10.1016/j.ecoinf.2022.101919>.
- Tam, A.Y., So, B.P., Chan, T.T., Cheung, A.K., Wong, D.W., Cheung, J.C., 2021. A blanket accommodative sleep posture classification system using an infrared depth camera: A deep learning approach with synthetic augmentation of blanket conditions. *Sensors* <http://dx.doi.org/10.3390/s21165553>.
- Vandad, D., Monet, S., Ali, E., 2020. Deep multitask learning for pervasive BMI estimation and identity recognition in smart beds. *J. Ambient Intell. Humaniz. Comput.* (Prepublish).

- Verhaert, V., Druyts, H., Van Deun, D., Exadaktylos, V., Verbraecken, J., Vandekerckhove, M., Vander Sloten, J., 2012. Estimating spine shape in lateral sleep positions using silhouette-derived body shape models. *Int. J. Ind. Ergon.* 42 (5), 489–498. <http://dx.doi.org/10.1016/j.ergon.2012.08.002>.
- Verhaert, V., Haex, B., De Wilde, T., Berckmans, D., Vandekerckhove, M., Verbraecken, J., Sloten, J.V., 2011a. Unobtrusive assessment of motor patterns during sleep based on mattress indentation measurements. *IEEE Trans. Inf. Technol. Biomed.* 15 (5), 787–794. <http://dx.doi.org/10.1109/TITB.2011.2131670>.
- Verhaert, V., Haex, B., De Wilde, T., Berckmans, D., Verbraecken, J., de Valck, E., Vander, S.J., 2011b. Ergonomics in bed design: The effect of spinal alignment on sleep parameters. *Ergonomics* 54 (2), 169–178. <http://dx.doi.org/10.1080/00140139.2010.538725>.
- Verhaert, V., Van Deun, D., Verbraecken, J., Vandekerckhove, M., Exadaktylos, V., Haex, B., Vander Sloten, J., 2013. Smart control of spinal alignment through active adjustment of mechanical bed properties during sleep. *J. Ambient Intell. Smart Environ.* 5 (4), 369–380. <http://dx.doi.org/10.3233/AIS-130216>.
- Wang, S., Huang, L., Jiang, Du, Sun, Y., Jiang, G., Li, J., Cejing Zou, H.F.Y.X., 2022. Improved multi-stream CBAM for sEMG-based gesture recognition. *Front. Bioeng. Biotechnol.* <http://dx.doi.org/10.3389/fbioe.2022.909023>.
- Xia, D.X., Su, S.Z., Geng, L.C., Wu, G.X., Li, S.Z., 2016. Learning rich features from objectness estimation for human lying-pose detection. *Multimedia Syst.* 23 (4), 515–526. <http://dx.doi.org/10.1007/s00530-016-0518-5>.
- Xu, X., Lin, F., Wang, A., Hu, Y., Huang, M., Xu, W., 2016. Body-earth mover's distance: A matching-based approach for sleep posture recognition. *IEEE Trans. Biomed. Circuits Syst.* 10 (5), 1023–1035. <http://dx.doi.org/10.1109/TBCAS.2016.2543686>.
- Yan, G., Woźniak, M., 2022. Accurate key frame extraction algorithm of video action for aerobics online teaching. *Mob. Netw. Appl.* 27 (3), 1252–1261. <http://dx.doi.org/10.1007/s11036-022-01939-1>.
- Yang, Z., Du, J., Sun, Y., Tao, B., Tong, X., Jiang, G., Kong, J., 2021. Dynamic gesture recognition using surface EMG signals based on multi-stream residual network. *Front. Bioeng. Biotechnol.* <http://dx.doi.org/10.3389/fbioe.2021.779353>.
- Yu, N., Yu, C., Li, H., Li, M., 2021. Effects of mattress firmness on infant body pressure distribution. *Int. J. Ind. Ergon.* 83, 103101. <http://dx.doi.org/10.1016/j.ergon.2021.103101>.
- Yu-Chi, L., Chih-Yun, L., Mao-Jiun, W., 2020. Better combination of thickness and hardness of mattress topper for supine sleeping posture: A physiological measurements evaluation. *Int. J. Ind. Ergon.* 78, 102979. <http://dx.doi.org/10.1016/j.ergon.2020.102979>.
- Yun, J., Jiang, D., Liu, Y., Sun, Y., Tao, B., Kong, J., Fang, Z., 2022. Real-time target detection method based on lightweight convolutional neural network. *Front. Bioeng. Biotechnol.* 10, 861286. <http://dx.doi.org/10.3389/fbioe.2022.861286>.
- Zhao, A., Dong, J., Zhou, H., 2020. Self-supervised learning from multi-sensor data for sleep recognition. *IEEE Access* 8, 93907–93921. <http://dx.doi.org/10.1109/ACCESS.2020.2994593>.